Kinetic Stabilization of an Oligomeric Protein under Physiological Conditions Demonstrated by a Lack of Subunit Exchange: Implications for Transthyretin Amyloidosis†

R. Luke Wiseman, Nora S. Green,‡ and Jeffery W. Kelly*

The Department of Chemistry and the Skaggs Institute of Chemical Biology, The Scripps Research Institute, 10550 North Torrey Pines Road BCC 265, La Jolla, California 92037

Received February 24, 2005; Revised Manuscript Received April 25, 2005

ABSTRACT: Kinetic stabilization of transthyretin (TTR) is established to prevent human neurodegeneration. Therefore, small molecule-mediated kinetic stabilization of the native state is an attractive strategy to prevent the misfolding and misassembly associated with TTR amyloid disease. Since the physiological microenvironment resulting in human TTR amyloidogenesis remains unclear, the conservative approach is to identify inhibitors that function under a variety of conditions. Small molecule kinetic stabilization of TTR has been established by concentration-dependent inhibition of acid-mediated amyloidogenesis and urea-induced tetramer dissociation. Since denaturing conditions reduce the binding affinity of inhibitors making it difficult to predict inhibitor efficacy under physiological conditions, we introduce a method for quantifying kinetic stabilization under physiological conditions. The rate of subunit exchange between wild-type TTR homotetramers and wild-type TTR homotetramers tagged with an N-terminal acidic flag tag is dictated by the rate of tetramer dissociation to its monomeric subunits prior to reassembly, rendering this method ideally suited for assessing the kinetic stabilization of TTR imparted by small molecule binding and evaluating small molecule binding constants. Addition of amyloidogenesis inhibitors to this exchange reaction slows tetramer dissociation in a concentration-dependent manner, stopping dissociation at concentrations where at least one inhibitor is bound to each tetramer in solution. Subunit exchange enables the rate of tetramer dissociation and the kinetic stabilization imparted by small molecule binding to be evaluated under physiological conditions in which the TTR concentration is not reduced by aggregation or irreversible dissociation.

Transthyretin (TTR)[1] is a 55-kDa homotetrameric protein that functions as a transporter of thyroxine and holo-retinol binding protein in the blood and cerebral spinal fluid (*1*). Extracellular deposition of TTR as amorphous aggregates and amyloid fibrils is genetically and biochemically linked to a number of human diseases characterized by nervous system or organ dysfunction. Deposition of wild-type TTR in cardiac tissue results in senile systemic amyloidosis (SSA) affecting 10% of the population over age 80 (*2*), while >100 destabilizing point mutations predispose individuals to TTR diseases, including familial amyloid polyneuropathy (FAP), familial amyloid cardiomyopathy (FAC), and central nervous system selective amyloidosis (CNSA) (*3*−*7*). The only therapeutic strategy currently available to ameliorate FAP is liver transplantation, in which a liver secreting a pathological TTR variant into the serum is replaced by a liver producing wild-type TTR. This therapy is expected to be ineffective for treating SSA and CNSA (TTR subject to misfolding in CNSA is secreted by the choroid plexus) and has also been found to be ineffective for treating some forms of FAP involving mutations other than V30M (*8*−*10*).

New therapeutic strategies are being developed that take advantage of our current understanding of the mechanism of TTR amyloidogenesis. Tetramer dissociation to a misfolded monomeric subunit is rate-limiting for amyloid formation in vitro and most likely in vivo (*11*−*13*). Increasing the kinetic barrier associated with TTR dissociation, referred to as kinetic stabilization, is known to prevent the TTR amyloid disease FAP. This knowledge comes from studies of a compound heterozygous family in Portugal having one TTR allele encoding the pathogenic mutation V30M, while the other encodes a T119M variant, which prevents the development of V30M FAP (*14*). Incorporating T119M subunits into TTR tetramers otherwise composed of disease-associated (V30M) subunits raises the dissociation barrier for tetramer dissociation through destabilization of the dissociative transition state, preventing tetramer dissociation and subsequent amyloidogenesis (*15*, *16*). Kinetic

† This work was supported in part by NIH Grants DK46335, the Skaggs Institute for Chemical Biology, the Lita Annenberg Hazen Foundation, the Norton B. Gilula Fellowship (R.L.W.), the Fletcher Jones Foundation Fellowship (R.L.W.), and NRSA Grant DK060304-03 (N.S.G.).

* Corresponding author. E-mail: jkelly@scripps.edu; phone: (858) 784-9601; fax: (858) 784-9610.

‡ Current address: Department of Chemistry, Randolph-Macon College, Box 5005, Ashland, VA 23005.

[1] Abbreviations: TTR, transthyretin; TTR·I, transthyretin bound by one small molecule amyloidogenesis inhibitor; TTR·I_2, transthyretin bound by two small molecule amyloidogenesis inhibitors; FAP, familial amyloid polyneuropathy; FAC, familial amyloid cardiomyopathy; CNSA, central nervous system amyloidosis; DMSO, dimethyl sulfoxide; ITC, isothermal titration calorimetry.

10.1021/bi050352o CCC: $30.25
Published on Web 06/02/2005

stabilization of TTR can also be mediated by selective small molecule binding to and stabilization of the native tetramer relative to the dissociative transition state (*16*). These amyloidogenesis inhibitors bind to one or both of the thyroxine binding sites within the TTR tetramer, imposing kinetic stabilization on the native state (*16*−*23*). One of the amyloidogenesis inhibitors discovered by screening, diflunisal, is currently being tested in a placebo-controlled clinical trial for the treatment of FAP, whereas another inhibitor, developed by structure-based drug design, will soon be tested in a clinical trial for FAC.

Small-molecule-mediated kinetic stabilization of TTR has been previously demonstrated by a decrease in the rate of tetramer dissociation under denaturing conditions (low pH or urea) (*16*). Unfortunately, the use of denaturing conditions makes it very difficult to choose the most effective small molecule kinetic stabilizers for use under physiological conditions because denaturing conditions are known to differentially alter inhibitor binding constants to TTR. Moreover, denaturing conditions lead to TTR depletion either by aggregation (low pH) (*12*) or by irreversible unfolding (high urea concentrations) (*11*), which temporally change the small molecule inhibitor to TTR tetramer ratio, making it difficult to discern the inhibitor stoichiometry required to prevent tetramer dissociation. An evaluation of the kinetic stabilization of TTR imposed by small molecule binding under physiological conditions would result in an additional ranking of amyloidogenesis inhibitors within a given chemical series. Moreover, this ranking may be highly relevant as there is experimental support for the hypothesis that TTR forms amyloid slowly at neutral pH in the extracellular space of humans (*24*−*27*).

Herein, we show that the rate of tetramer dissociation can be conveniently evaluated by measuring the rate at which wild-type TTR homotetramers and N-terminally labeled flag-tag wild-type TTR homotetramers exchange subunits under physiological (nondenaturing) conditions utilizing anion exchange chromatography (Figure 1) (*28*). Previously, it has been demonstrated that the addition of the flag-tag sequence to the N-terminus of TTR does not affect the kinetic or thermodynamic stability of the TTR tetramer (*28*). Rate-limiting tetramer dissociation, followed by the rapid reassembly of monomeric subunits into tetramers **1**−**5** enable subunit exchange (Figure 1). Addition of known TTR amyloidogenesis inhibitors to the exchange reaction decreases the rate of subunit exchange in a concentration-dependent manner, demonstrating kinetic stabilization. The subunit exchange method is useful for rank ordering the efficacy of the small molecule kinetic stabilizers under physiological conditions and for checking their experimentally determined binding constants.

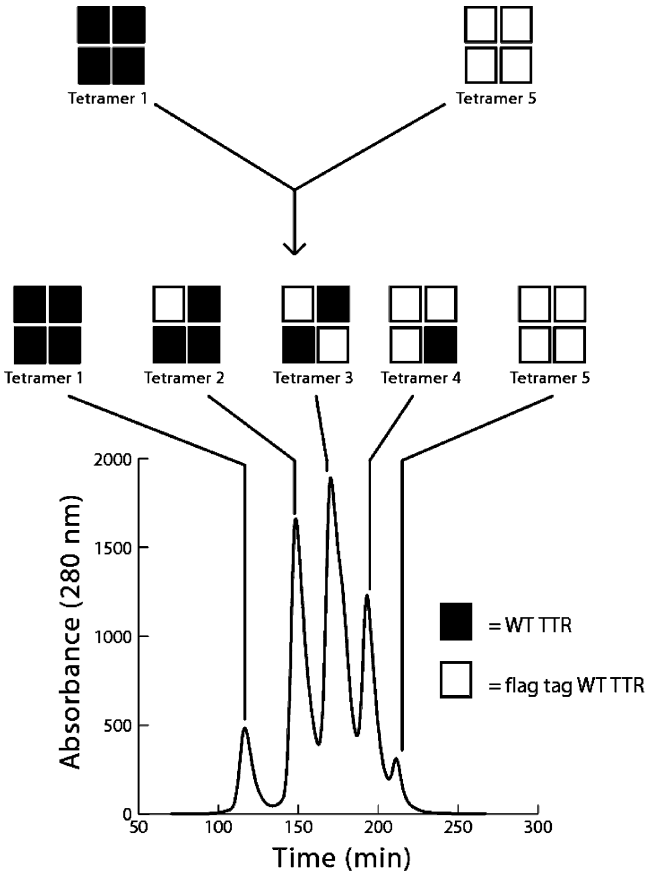

FIGURE 1: Mixing homotetrameric wild-type TTR (tetramer **1**) and homotetrameric flag-tag wild-type TTR (tetramer **5**) results in a time-dependent exchange of subunits affording tetramers **1**−**5**. The kinetics of the exchange process can be followed until the monomeric subunits are statistically distributed among tetramers **1**−**5**. The chromatogram demonstrates that tetramers **1**−**5** can be separated on an anion exchange column, allowing quantification of the extent of exchange as a function of time.

MATERIALS AND METHODS

Expression and Purification of Wild-Type TTR and Flag-Tag Wild-Type TTR. Both wild-type TTR and flag-tag wild-type TTR were prepared as previously described (*28*, *29*). Briefly, both wild-type and flag-tag wild-type TTR were expressed in BL21 *Escherichia coli*. Selection was performed in Luria-Bertani broth with 100 μg/mL ampicillin (wild-type TTR) or 150 μg/mL kanamycin (flag-tag wild-type TTR). 1 mM IPTG was added to the cells when an OD_{600nm} of 0.8−1.0 was achieved. Cells were lysed with three rounds of sonication at 4 °C, and the supernatant was collected following centrifugation. The supernatant was then treated with a 50% ammonium sulfate and then collected following centrifugation. TTR was precipitated by centrifugation following a 50−90% ammonium sulfate treatment. The protein was then dialyzed overnight into 25 mM Tris pH 8.0, 1 mM EDTA with 7000 MW dialysis tubing (Snakeskin from Pierce Biomedical). TTR was purified first on a Source15Q anion exchange column (Amersham Biosciences) eluting with either a 200−350 mM NaCl gradient (wild-type TTR) or a 200−500 mM NaCl gradient (flag-tag wild-type TTR) at 4 °C. The TTR was further purified by gel filtration chromatography using a Superdex 75 column (Amersham Biosciences; 50 mM sodium phosphate pH 7.2, 100 mM KCl, 1 mM EDTA). The protein was identified by LC-MS analysis (Hewlitt-Packard 1100-MSD mass spectrometer; wild-type TTR − 13890; flag-tag wild-type TTR − 15880).

Subunit Exchange of Wild-Type TTR and Flag-Tag Wild-Type TTR. Homotetrameric wild-type TTR and homotetrameric flag-tag wild-type TTR were prepared at the desired concentrations (0.1, 1, or 20 μM; 50 mM sodium phosphate pH 7.2, 100 mM KCl, 1 mM EDTA). The proteins were mixed in equal volumes into an eppendorf tube and incubated at 25 °C for the indicated times. Subunit exchange was

followed using a SMART system equipped with a μPeak monitor and a Mono Q PC 1.6/5 column, as previously described (*28*). A total of 50 μL of the exchange reaction was added to the SMART system running a gradient of 240−420 mM NaCl in 25 mM Tris pH 8.0, 1 mM EDTA. Because the flag-tag provides ~6 negative charges to each tagged TTR subunit (pH 7), the more flag-tag TTR subunits in the tetramer the longer the retention time on the anion exchange column. Integration of the observed UV curves was performed using SMART Manager 1.41 software according to the manager's instructions. The extent of exchange was calculated by dividing the integration of the specific tetramer by the total integration determined for all of the tetramers. The fraction exchange was calculated using the predicted statistical distribution of the various stoichiometries at the end of the exchange reaction (tetramers **1** and **5**: [1 − (extent of exchange − 0.0625)/(0.50 − 0.0625)]; tetramers **2** and **4**: [extent of exchange/0.25]; tetramer **3**: [(extent of exchange)/0.375]). The reported rate constants of exchange were determined from plotting the fraction exchange data in Kaleidograph and fitting the results to a first-order single-exponential kinetic equation.

Modeling of Subunit Exchange in the Presence of Small Molecules. Mathematical modeling was performed using Mathematica 5.0 on a Dell Inspiron 4000 with an Intel Pentium III processor utilizing 256 MB of RAM. The rate equations (Supporting Information) defining the species depicted in Figure 3A were simultaneously solved using the NDSOLVE function. The initial concentrations of tetramer **1** and tetramer **5** were varied from 0.1 to 20 μM, as indicated in the text. Similarly, the total ligand concentration was varied from 0 to 2 μM as indicated. The thermodynamic binding constants for small molecule binding to the TTR tetramer were varied by changing k_{off1} and k_{off2} to the appropriate value according to the equation $K_1 = k_{on1}/k_{off1}$ and $K_2 = k_{on2}/k_{off2}$, using $k_{on1} = k_{on2} = 10^7$ M^{-1} s^{-1}.

Small Molecule Inhibition of Subunit Exchange. Small molecules were added to both homotetrameric TTR solutions (wild-type TTR and flag-tag wild-type TTR) at the indicated concentrations from a 1 mM solution of the appropriate small molecule in DMSO. The homotetrameric solutions were then mixed to commence subunit exchange and analyzed as above.

Correlation between Unbound Protein and the Observed Rate Constant of Subunit Exchange. The population of unbound, singly bound, and doubly bound TTR as a function of the concentration of **6** was calculated using the previously reported binding constants determined by isothermal titration calorimetry. The observed rate constant of subunit exchange for the various concentrations of **6** was calculated as above. The plot was prepared in Kaleidograph fitting the data representing the dependence of the observed rate constant of subunit exchange (k_{app}) and the mole fraction of tetrameric species to a line with an equation of log [species] = 1.0588 log k_{app} − 4.2498 with an $R^2 = 0.99603$.

Similarly, the population of unbound TTR tetramers for varying concentrations of **7**−**9** was calculated using the previously reported binding constants. The plot of log-[unbound tetramer] versus log k_{app} was prepared as above yielding a line with an equation of log[species] = 0.74119 log k_{app} − 4.9028 with an $R^2 = 0.95552$.

RESULTS

Subunit Exchange between TTR Tetramers Requires Dissociation Followed by Mixing of Monomeric Subunits upon Reassembly. Before subunit exchange can be used to evaluate kinetic stabilization, its mechanism must be understood. Measuring the rate of appearance/disappearance for tetramers **1**−**5**, from mixtures of homotetramers **1** and **5**, provides the means to discern whether dissociation of tetramers to monomers is required for subunit exchange and/or whether other intermediates, such as dimers, are capable of enabling subunit exchange. The rate of exchange between subunits of the wild-type TTR homotetramer (tetramer **1**) and flag-tag wild-type TTR homotetramer (tetramer **5**) was evaluated by mixing equal volumes of tetramer **1** (1 μM) and tetramer **5** (1 μM; 25 °C). The distribution of tetramers **1**−**5** was followed as a function of time by anion exchange chromatography (Figure 1). As subunit exchange proceeds, the population of mixed tetramers **2**−**4** increases, while the population of tetramers **1** and **5** decreases (Figure 1; tetramer **2**: (wild-type TTR)$_3$(flag-tag wild-type TTR)$_1$; tetramer **3**: (wild-type TTR)$_2$(flag-tag wild-type TTR)$_2$; tetramer **4**: (wild-type TTR)$_1$(flag-tag wild-type TTR)$_3$). The kinetics of subunit exchange can be fit to a first-order rate equation, from which a rate constant of subunit exchange (k_{ex}) can be extracted. The rates at which tetramers **1** and **5** disappear and **2**−**4** appear are nearly identical, as indicated by determination of a rate constant for each time course (tetramer **1** $k_{ex} = 0.027 \pm 0.004$ h^{-1}; tetramer **2** $k_{ex} = 0.028 \pm 0.01$ h^{-1}; tetramer **3** $k_{ex} = 0.026 \pm 0.005$ h^{-1}; tetramer **4** $k_{ex} = 0.027 \pm 0.003$ h^{-1}; tetramer **5** $k_{ex} = 0.026 \pm 0.005$ h^{-1}; $n = 9$; in the presence of 0.1% DMSO), suggesting that TTR must fully dissociate to monomeric subunits prior to reassembly (Figure 2A). If homotetrameric TTR dissociated to a stable intermediate capable of reassembly into a tetramer, such as a dimer, one would expect to see different rates of exchange for tetramers **1**−**5**, which was not observed (Figure 2A). Furthermore, the final amplitude of the observed exchange corresponds with the predicted statistical distribution of tetramers (1:4:6:4:1 for tetramers **1**−**5**, respectively; Figure 2A, dashed lines).

Tetramer Dissociation Is Rate-Limiting for Subunit Exchange between Wild-Type TTR and Flag-Tag Wild-Type TTR. The rate of subunit exchange was measured over a 200-fold change in total TTR concentration (0.1, 1, and 20 μM) to evaluate the dependence of the kinetics of subunit exchange on the total concentration of protein (Figure 2B). The amplitude-normalized subunit exchange profiles for all concentrations of equimolar mixtures of tetramers **1** and **5** were found to be identical, demonstrating first-order kinetics (Figure 2B). These data strongly suggest that tetramer dissociation, which also exhibits first-order kinetics, is rate-limiting for subunit exchange at pH 7.0, implying that the process required to reassemble the monomers to tetramers **1**−**5** is fast relative to tetramer dissociation. This hypothesis is consistent with the previously reported time scales of TTR tetramer dissociation ($t_{1/2}$ = 42 h) (*11*) and tetramer reassembly (complete within seconds) (*6*, *11*). Notably, the rate constant for subunit exchange, $k_{ex} = 0.027$ h^{-1}, is very similar to the reported rate constant for TTR tetramer dissociation ($k_{diss} = 0.0168 \pm 0.0015$ h^{-1}). The 2-fold difference is not surprising considering that the reported k_{diss} at 0 M urea (pH

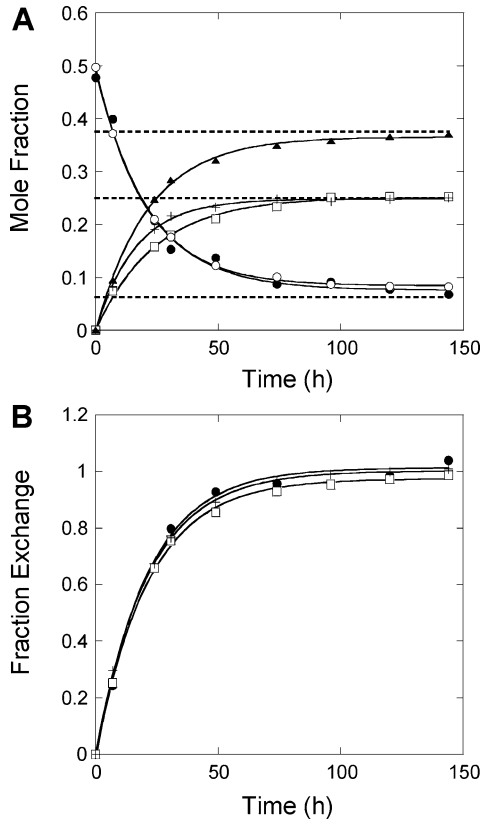

FIGURE 2: The rate of subunit exchange is governed by the rate of TTR tetramer dissociation. (A) The time course of subunit exchange was measured by following the appearance/disappearance of peaks corresponding to tetramers **1**−**5** on the anion exchange chromatogram. The rate constant for the disappearance of **1** and **5** is identical to the rate constant for the appearance of **2**−**4**, consistent with the complete dissociation of the tetramers to monomers prior to reassembly. The dashed lines represent the predicted statistical distribution of tetramers **1**−**5** upon completion of the subunit exchange reaction. Tetramer **1**: filled circles, tetramer **2**: open squares, tetramer **3**: filled triangles, tetramer **4**: crosses, and tetramer **5**: open circles. (B) The amplitude-normalized time course of the appearance of tetramer **3** initiated by mixing equal volumes and concentrations of tetramers **1** and **5** giving a final concentration of 0.1 μM (filled circles), 1 μM (open squares), and 20 μM (crosses) TTR. The normalized rate of subunit exchange is independent of the protein concentration because tetramer dissociation is rate-limiting.

7.0) was derived by an extrapolation of k_{diss} from urea solutions (6.0 to 8.0 M) (*11*). Collectively, these data support the conclusion that the rate of subunit exchange is limited by the rate of tetramer dissociation; hence, the slow tetramer dissociation step can be monitored under physiological conditions using subunit exchange.

Subunit Exchange Can Be Mathematically Modeled. A mathematical model describing subunit exchange in the presence of small molecule inhibitors was prepared using the mechanistic insights discussed above (Figure 3A; Supporting Information). The model utilizes rate constants associated with the processes of tetramer dissociation (k_{diss}) and tetramer assembly (k_a). The tetramer dissociation rate constant used in the model was that determined experimentally for the exchange of wild-type TTR and flag-tag wild-type TTR in the presence of 0.1% DMSO, the vehicle used for small molecule addition ($k_{diss} = k_{ex} = 0.026$ h^{-1}), a rate constant within a factor of 2 of k_{diss} measured experimentally by extrapolation from urea solutions. Since the mechanism of tetramer assembly is unknown, the assembly of TTR tetramers from monomeric subunits was assumed to occur by a spontaneous and very rapid ($k_a = 10^{20}$ M^{-3} s^{-1}) fourth-order association process. To take into account the statistical distribution of tetramers **1**−**5**, after completion of the exchange reaction, the assembly rate constant for each tetramer was multiplied by a factor representing the predicted statistical distribution (tetramers **1** and **5**: 1/16; tetramers **2** and **4**: 4/16; and tetramer **3**: 6/16). Initial concentrations of tetramers **1**−**5** were written directly into the algorithm to allow for variations in concentration of total protein, which amounts to tetramer **1** + tetramer **5** at $t = 0$ h. The model accurately predicts that the rate constant of subunit exchange is not concentration dependent when varying the total protein from 0.1 to 20 μM, yielding the expected exchange rate constant (k_{ex}) identical to that of k_{diss} (Figure 3B; $k_{ex} = 0.026$ h^{-1}). Furthermore, the appearance/disappearance of tetramers **1**−**5** are observed to vary at the same rate, reaching a steady-state at the predicted statistical distribution of subunits (Figure 3C).

Ligand binding was also included into the subunit exchange model to predict the effectiveness of ligands with different binding constants on the subunit exchange process (Figure 3A). Small molecule binding was included utilizing rate constants for ligand binding to the first and second TTR binding sites (k_{on1} and k_{on2}, respectively) and ligand dissociation rate constants from the first and second binding sites of the TTR tetramer (k_{off1} and k_{off2}, respectively; Figure 3A). The rate constants used for small molecule binding to the two thyroxine binding sites (k_{on1} and k_{on2}) were set to 10^7 M^{-1} s^{-1}, which corresponds with experimentally determined rate constants for ligand binding to the TTR tetramer (P. Hammarström, R. L. Wiseman, and J. W. Kelly, unpublished results) and is similar to known binding rate constants for protein−ligand interactions (*30*). The rate constants of ligand dissociation, k_{off1} and k_{off2}, were dictated by the experimentally determined binding constants, K_1 and K_2, and the rate constants of ligand binding ($k_{off1} = 10^7$ M^{-1} s^{-1}/ K_1; $k_{off2} = 10^7$ M^{-1} s^{-1}/K_2). Initial ligand concentration was written into the model directly to evaluate the dependence of the rate of subunit exchange on the concentration of different amyloidogenesis inhibitors.

Inhibition of Subunit Exchange by Small Molecule Binding Reveals that Only TTR But Not TTR·I or TTR·I$_2$ Can Undergo Tetramer Dissociation and Subunit Exchange. To evaluate the effects of ligand binding on the tetramer dissociation rate reflected by the rate of subunit exchange, varying concentrations of a known amyloidogenesis inhibitor, compound **6** (Figure 4), were incubated with homotetrameric wild-type TTR and homotetrameric flag-tag wild-type TTR prior to mixing them to initiate the exchange reaction (Figure 5A; 25 °C; pH 7.0). As the concentration of **6** was increased from 0 to 2 μM ([TTR]$_{Total}$ = 1 μM), the apparent first-order rate constant for subunit exchange, k_{app}, decreased (Table 1), demonstrating an inverse relationship between the concentration of small molecule and the rate of exchange (Figure 5A). Long-term incubation (>1000 h) of the exchange reaction in the presence of **6** (2 μM; Figure 5A open circles displays only the early time course) shows that the reaction eventually proceeds to completion, albeit much more slowly than in the absence of **6** (data not shown). These data directly demonstrate that **6** kinetically stabilizes the

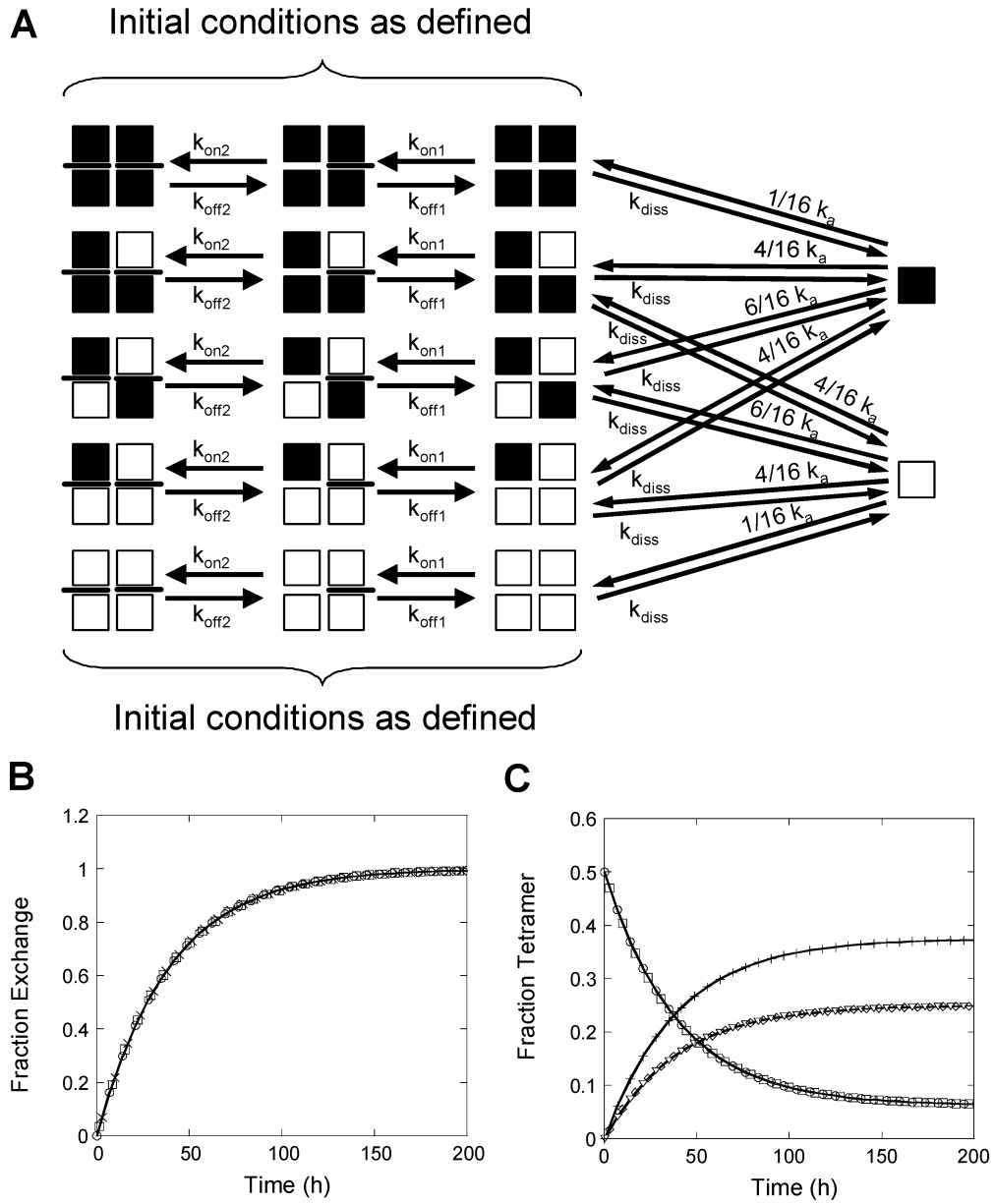

FIGURE 3: A mathematical model can be developed that accurately predicts the subunit exchange reaction. (A) Overview of the inputs to the model used to predict the effect of small molecule inhibitors on the subunit exchange reaction. A detailed description of the model along with the mathematical code employed can be found in the Supporting Information. Briefly, the model is defined by the rate constants of tetramer dissociation (k_{diss}), tetramer assembly (k_a), and ligand binding (k_{on1}, k_{on2}, k_{off1}, k_{off2}). To vary the protein or ligand concentrations, the initial conditions were defined by entering the concentrations of the various species at $t = 0$ h. (B) Mathematically derived amplitude normalized subunit exchange rates for 0.1 (circles), 1 (squares), and 20 (crosses) μM TTR as indicated by measuring the appearance of tetramer **3**. Subunit exchange displays the same first-order kinetics regardless of the total protein concentrations, in agreement with the experimental results. (C) Mathematically derived exchange rates for tetramers **1**−**5** calculated using the above model (A). All of the tetrameric species appear/disappear with the same first-order kinetics, in agreement with the experimentally observed results. Tetramer **1**: circles; tetramer **2**: upside down triangle; tetramer **3**: crosses; tetramer **4**: diamonds; tetramer **5**: squares.

native TTR tetramer, decreasing the rate of tetramer dissociation. Utilizing the mathematical model outlined in Figure 3A and K_1 and K_2 determined by isothermal titration calorimetry (ITC) (*21*) (Figure 4) demonstrates that the experimental data (Figure 5A symbols) can be very accurately predicted by the model system (Figure 5A, black lines; $R^2 > 0.99$ in all cases, Table 1).

The populations of unbound (T), singly bound (T·**6**), and doubly bound (T·$\mathbf{6}_2$) TTR tetramers were calculated for several concentrations of **6**, using the previously determined binding constants. Plotting the log of the concentration of the various tetrameric species versus the log of k_{app} reveals a linear correlation between T and the observed rate constant of subunit exchange (Figure 5B). The log of k_{app} did not display a linear correlation with either T·**6** or T·$\mathbf{6}_2$, implying that these species are not responsible for measurable subunit exchange. Calculating k_{app} determined from the model under identical conditions displays a similar linear correlation with the concentration of T, resulting in a line with a slope nearly identical to that yielded by the experimental results (data not shown). The strong correlation between k_{app} and T but not T·**6** or T·$\mathbf{6}_2$ as a function of the concentration of **6** suggests that neither T·**6** or T·$\mathbf{6}_2$ are able to undergo tetramer dissociation on a biologically relevant time scale (Figure 5C).

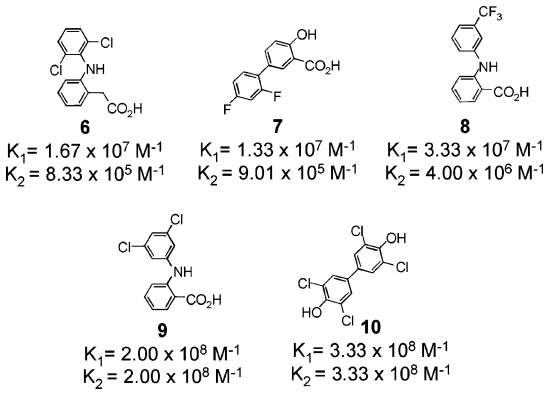

FIGURE 4: Structures of the small molecule inhibitors **6**−**10**. The thermodynamic binding constants, determined from isothermal titration calorimetry analysis, are indicated.

Therefore, k_{app} is dependent not only on the inherent rate constant of tetramer dissociation (k_{diss}) but also on the ligand concentration and the thermodynamic binding constants of the small molecule amyloidogenesis inhibitors to each thyroxine binding site. These data corroborate recently published studies demonstrating that binding of a small molecule to one of the two T_4 binding sites is sufficient to impose kinetic stabilization on the entire TTR tetramer (*31*, *32*).

Other Established Small Molecule Amyloidogenesis Inhibitors also Kinetically Stabilize the TTR Tetramer against Subunit Exchange under Nondenaturing Conditions. To demonstrate the generality of small molecule inhibition of subunit exchange, wild-type TTR (tetramer **1**; 1 μM) and flag-tag wild-type TTR (tetramer **5**; 1 μM) were preincubated with small molecules **7**−**10** (1 or 2 μM; Figure 6A−D) and mixed to initiate subunit exchange, monitoring the exchange reaction by anion exchange chromatography (25 °C; pH 7.0). Because **7**−**10** display different binding constants and binding cooperativities for the two thyroxine binding sites (Figure 4), one could expect to observe a different inhibitor efficacy from the subunit exchange analyses (*16*, *33*). Compounds **7**−**9** inhibit subunit exchange similarly to **6** (Figure 6A−C). Preincubation of **7**−**9** (1 μM; $[TTR]_{total}$ = 1 μM) resulted in a decrease in the rate of subunit exchange. All of these samples completely exchanged subunits after long-term incubation (>1000 h; data not shown). Increasing the concentration of **7**−**9** to 2 μM dramatically reduced the rate of subunit exchange (Figure 6A−C). However, compounds **7** and **8** still allow very slow subunit exchange, achieving complete exchange only after long incubation periods (>2000 h; data not shown), unlike compound **9** which completely prevented subunit exchange under these conditions (Figure 6C).

Applying the mathematical model of subunit exchange (as accomplished above for **6**) to inhibitors **7** and **8** using the experimentally determined binding data (*16*, *21*) demonstrates that the experimentally observed inhibition of exchange (Figure 6A,B; symbols) is very similar to the predicted inhibition of tetramer dissociation and subunit exchange (Figure 6A,B; black lines). Compounds **7** and **8** do perform slightly better than predicted, which can be attributed to experimental error in the determination of the binding constants and the experimental error in subunit exchange analysis. The predicted inhibition of subunit exchange by **9**, based on the previously reported thermodynamic binding constants (Figure 6C; black lines), significantly underestimates the experimentally observed inhibition when **9** is studied at 1 μM (*16*). Since the experimentally determined binding constants for **9** are at the upper limit of sensitivity for traditional ITC (*34*), it is reasonable to assume that the actual binding constants for **9** are higher than previously thought. Varying the binding constants of **9** increases the accuracy of the fit. The mathematical model

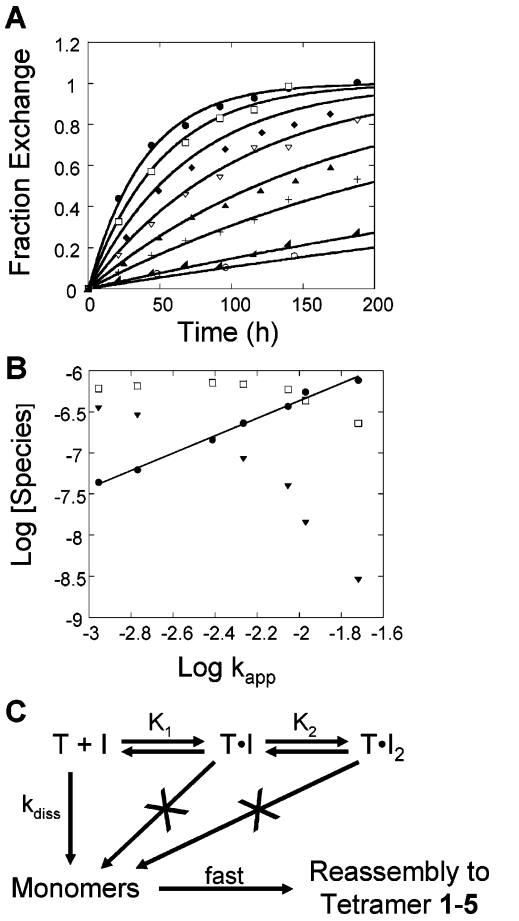

FIGURE 5: The extent of subunit exchange, as a function of time, allowed by inhibitor **6** can be directly correlated with the amount of unliganded TTR tetramer in the subunit exchange reaction. (A) Time course of subunit exchange (measuring the appearance of tetramer **3**; total TTR = 1 μM) as a function of the concentration of **6**. The symbols represent the experimental results, whereas the solid lines represent the predicted rate of exchange according to the mathematical model of subunit exchange. The R^2 values of the predicted fit can be found in Table 1. Control (TTR in the absence of **6**) filled circles; 0.25 μM **6**: open squares; 0.5 μM **6**: filled diamonds; 0.75 μM **6**: open triangles; 1.0 μM **6**: filled triangles; 1.25 μM **6**: crosses; 1.75 μM **6**: filled wedges; 2.0 μM **6**: open circles. (B) Plot of the log of the various tetrameric species (unbound tetramer: filled circles; TTR·**6**: open squares; and TTR·$\mathbf{6}_2$: filled triangles) versus the log of k_{app} (measured by the appearance of tetramer **3**), representing the rate of subunit exchange in the presence of varying concentrations of **6**. The concentration of the tetrameric species was calculated from the binding constants of inhibitor **6** (Figure 4). Only the unliganded TTR tetramer concentration correlated with the rate of subunit exchange, demonstrating that only the unliganded TTR tetramers are capable of dissociating and undergoing subunit exchange. (C) Pictorial summary of (B) demonstrating that unliganded TTR and not TTR·**6** or TTR·$\mathbf{6}_2$ contribute to the observed dissociation and subsequent subunit exchange of the TTR tetramer. Unbound TTR tetramer: T; singly bound TTR tetramer: T·I; doubly bound TTR tetramer: T·I_2; rate of tetramer dissociation: k_{diss}; thermodynamic binding constants: K_1 and K_2.

Table 1: Apparent Rate Constants of Subunit Exchange (k_{app}) in the Presence of Varying Concentrations of **6** ([TTR]$_{total}$ = 1 μM)[a]

[**6**] (μM)	apparent rate constant (k_{app}; h^{-1})	R^2 value from model fit
0	0.026	0.997
0.25	0.019	0.998
0.5	0.011	0.995
0.75	0.0099	0.994
1.0	0.0054	0.998
1.25	0.0039	0.995
1.75	0.0017	0.979
2.0	0.0011	0.999

[a]Data from Figure 5A. The apparent rate constant (k_{app}) is not only dependent on the rate constant for tetramer dissociation (k_{diss}) but also on the ligand concentration and the thermodynamic binding constants of the inhibitors K_1 and K_2. The correlation between the experimental results and the predicted results from the mathematical model (presented in Figure 3A) is demonstrated by the favorable R^2 values for the different concentrations of **6**.

suggests that **9** binds with negative cooperativity where $K_1 = 2 \times 10^{10}$ M^{-1} and $K_2 = 1 \times 10^9$ M^{-1} (Figure 6C, dashed lines), in contrast to the previously determined binding constants for **9** determined by ITC (Figure 4).

The population of unbound tetramer in the presence of compounds **6**−**9** (0.5, 1.0, and 2.0 μM) was calculated using the reported binding constants determined by ITC (Figure 4). Plotting the log of the concentration of unbound TTR against the log of k_{app} demonstrates a linear dependence (Figure 7A), analogous to that observed for varying concentrations of **6** (Figure 5B). In contrast, plotting the log of either the singly bound tetramer (T·I) or the doubly bound tetramer (T·I_2) concentrations against the log of k_{app} does not exhibit a linear relationship (Figure 7B,C). Collectively, these data demonstrate that tetramer dissociation and subunit exchange can only proceed from T and not from either the singly bound tetramer (T·I) or the doubly bound tetramer (T·I_2).

Inhibition of TTR subunit exchange by inhibitor **10** was significantly different than the inhibition of exchange by **6**−**9**. Incubating **10** (1 μM) with TTR (1 μM) yields a value for k_{app} (0.021 h^{-1}) that is very similar to the control in the absence of inhibitor (control k_{ex} = 0.026 h^{-1}), while the amplitude of the observed exchange reaction was reduced to 40% of TTR without inhibitor (Figure 6D). Long-term incubation (>2400 h) of the subunit exchange reaction in the presence of **10** (1 μM) reveals that the reaction still slowly proceeds toward completion (data not shown). Increasing the concentration of **10** to 2 μM results in complete inhibition of subunit exchange (Figure 6D). Applying the mathematical model to the subunit exchange reaction, using the previously reported binding constants for **10** determined by ITC (Figure 4) (*22*), does not accurately predict the observed results (Figure 6D; black lines). However, we have reason to believe that the binding constants for **10** were significantly underestimated by ITC. Mass spectrometric analysis carried out in collaboration with Carol Robinson's lab reveals that **10** binds to the TTR tetramer with positive cooperativity, which would not be discernible by ITC (*35*). Modeling the inhibition of subunit exchange by **10** demonstrates that once $k_{off2} < k_{diss}$, the predicted inhibition profile for **10** (1 μM) is very similar to the experimental data (Figure 6D; dashed lines). Because the experimentally derived profile depends

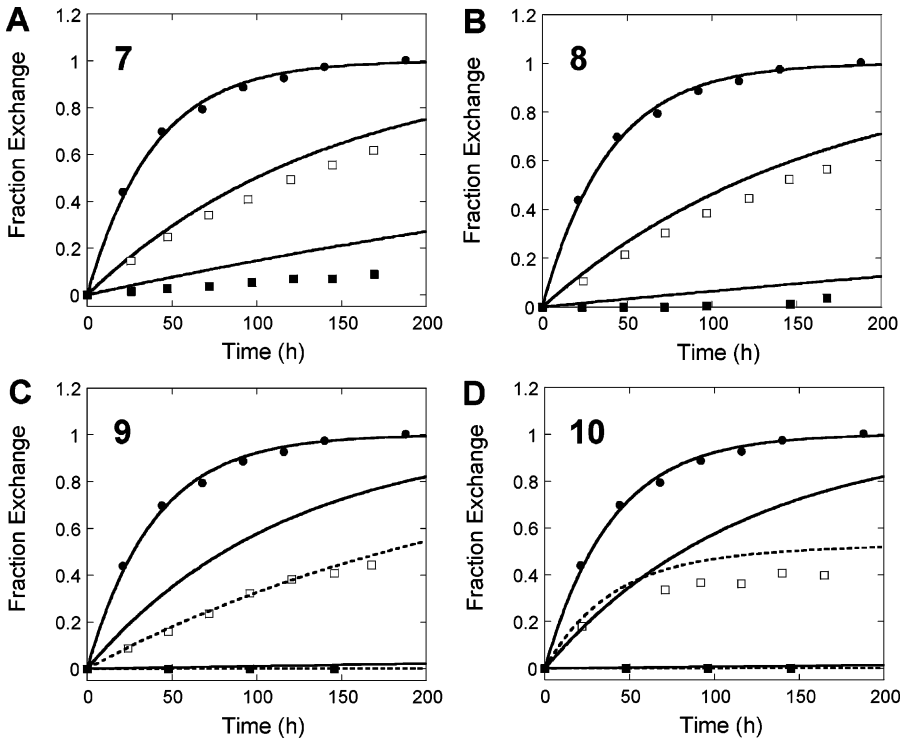

FIGURE 6: The extent of kinetic stabilization revealed by the time course of subunit exchange depends on the inhibitor binding constants and the inhibitor concentration. **A**−**D** Subunit exchange reaction in the presence of 1 or 2 μM inhibitor ([TTR]$_{total}$ = 1 μM; A: **7**; B: **8**; C: **9**, and D: **10**). The symbols (no inhibitor: filled circles; 1 μM inhibitor: open squares; 2 μM inhibitor: filled squares) represent the experimentally observed subunit exchange time course and the lines represent the mathematically predicted exchange rate, using the previously reported thermodynamic binding constants determined from ITC (Figure 4). The dashed lines in C and D represent a more accurate fit of the experimental data, achieved by varying the thermodynamic binding constants in the mathematical model.

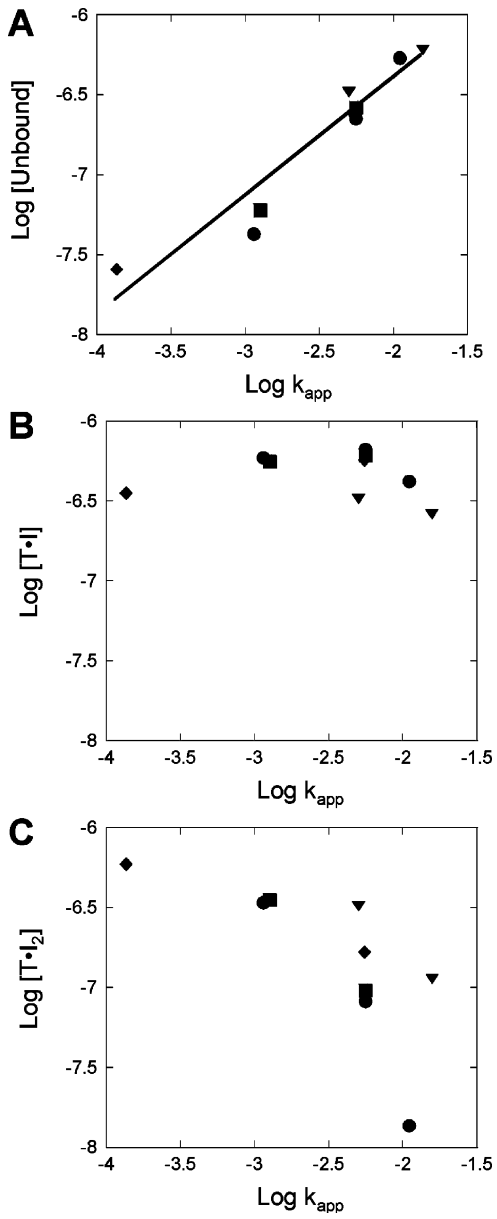

FIGURE 7: Plots of the log of the concentration of various tetrameric species [unbound tetramer (A); TTR•I (B); and TTR•I_2 (C)] versus the log of k_{app} (measured by the appearance of tetramer **3**), representing the rate of subunit exchange in the presence of varying concentrations of compounds **6**−**9**. **6**: circles; **7**: squares; **8**: diamonds; **9**: upside-down triangles. These plots demonstrate that the rate of subunit exchange best correlates with the concentration of unliganded TTR (line in A) and poorly with TTR•I (B) and TTR•I_2 (C). The concentration of the tetrameric species was calculated from the thermodynamic binding constants in each case (Figure 4).

primarily on k_{off2}, it is difficult to predict the binding constants for **10** binding to TTR, but these results suggest that binding displays very high affinity and positive cooperativity.

DISCUSSION

Small molecule-mediated kinetic stabilization of the TTR tetramer is an attractive therapeutic strategy to prevent and hopefully treat the TTR amyloidoses (*16*, *36*). Increasing the energetic barrier associated with tetramer dissociation is known to prevent TTR amyloid disease in compound heterozygotes expressing both the trans-suppressor subunit (T119M) and the FAP-associated subunit, V30M (*14*, *15*). Small molecule binding can also increase the energetic barrier for tetramer dissociation by selectively stabilizing the tetrameric ground state relative to the dissociative transition state (*16*). Since the small molecule strategy mimics the mechanism of trans-suppression, there is reason for optimism that these inhibitors will be effective for treating TTR amyloid disease.

Although kinetic stabilization, imposed by small molecule amyloidogenesis inhibitor binding, has been demonstrated utilizing denaturing conditions (low pH and high urea concentrations) (*16*−*18*, *23*), it is difficult to predict the efficacy of small molecule inhibitors under physiological conditions, owing to the influence of denaturing conditions on the inhibitor binding constants K_1 and K_2. Furthermore, since both acid-mediated aggregation and urea-mediated dissociation/unfolding assays continuously deplete the native TTR tetramer due to aggregation and dissociation/unfolding, respectively, the relative concentrations of unbound (T), singly bound (T•I), and doubly bound (T•I_2) TTR tetramers is constantly changing throughout each assay, further complicating the analysis of inhibitor efficacy. Last, the use of low pH and chaotropes to measure kinetic stabilization may not be physiologically relevant to amyloidogenesis of TTR in vivo. TTR amyloid deposits are observed in the extracellular space where the pH is near neutral; therefore, it is important to analyze the efficacy of small molecule kinetic stabilizers at a physiologically relevant pH.

Subunit exchange is an ideal method to evaluate the extent of kinetic stabilization imposed on the TTR tetramer by small molecule inhibitor binding. In contrast to other methods used to demonstrate kinetic stabilization, subunit exchange offers the ability to measure the tetramer dissociation rate at constant concentrations of small molecule and tetrameric TTR, i.e., under nondenaturing conditions. The subunit exchange method demonstrates that increasing the barrier for tetramer dissociation is achieved either by increasing the concentration of ligand or by using ligands with higher binding constants. Furthermore, the chromatographic method utilized to follow the kinetics of the exchange process in the presence of small molecule ligands is readily available in the majority of laboratories.

Subunit exchange also offers an opportunity to scrutinize previously determined inhibitor binding constants to TTR. Fitting the subunit exchange time courses over a range of ligand concentrations allows for the confirmation or determination of binding constants from a simple modeling analysis. We provide evidence that the binding constants for amyloidogenesis inhibitors **9** and **10** are slightly underestimated by ITC. This is not surprising considering that the measured binding constants were at the upper limit of ITC sensitivity. Subunit exchange modeling was even capable of substantiating the positive TTR binding cooperativity exhibited by **10**, previously suggested by mass spectrometric analysis, although the exact binding constants could not be estimated because of their magnitude. Using both the exchange model and the experimental subunit exchange profile at specific inhibitor concentrations, it is now possible to refine the thermodynamic binding constants of amyloidogenesis inhibitors to TTR.

Subunit exchange can also demonstrate that TTR tetramers bound by only one inhibitor cannot undergo tetramer

dissociation. It is established that TTR tetramers bound by two small molecule ligands are kinetically stabilized against dissociation (*16*, *17*); however, the denaturing conditions previously used to demonstrate this stabilization precludes drawing conclusions about the kinetic stability of T·I. We have recently shown with substantial effort that tethering a single small molecule amyloidogenesis inhibitor to the TTR tetramer is sufficient to kinetically stabilize the entire TTR tetramer, preventing dissociation under denaturing conditions (*32*). Because the tetramer to small molecule ratio does not vary under the conditions of the subunit exchange reaction, it is possible to demonstrate herein that singly bound TTR tetramers do not dissociate under physiological conditions without having to covalently tether the inhibitor to the TTR tetramer. Under all conditions studied, the apparent rate constant of subunit exchange, k_{app}, correlates only with the concentration of unliganded TTR tetramers (T). If singly bound TTR tetramers were capable of undergoing dissociation and subunit exchange, one would expect to observe a deviation from this linear relationship. The kinetic stability of T·I demonstrates that it is not necessary to form $T{\cdot}I_2$ to prevent tetramer dissociation, thus allowing lower doses of inhibitors to be used in clinical trials.

The promise of small molecule-mediated kinetic stabilization as a therapeutic strategy to prevent protein misfolding diseases has provided incentive for the development of methods to demonstrate kinetic stabilization under physiological conditions. Evaluating the rate of subunit exchange is an attractive strategy to demonstrate kinetic stabilization of oligomeric proteins. Assays based on subunit exchange rates could be used to identify small molecule kinetic stabilizers of oligomeric proteins, other than TTR, that misfold, such as superoxide dismutase whose dissociation and misfolding are associated with amyotrophic lateral sclerosis (ALS) (*37*). This strategy should not be limited to homooligomers but could also be used to identify small molecules that stabilize heterooligomeric complexes by measuring the exchange between tagged and untagged subunits. Such an approach could be useful for identifying small molecule stabilizers of heterodimeric complexes between huntingtin and huntingtin binding proteins, providing an opportunity to stabilize the huntingtin protein whose misfolding appears to be associated with Huntington's disease (*38*).

Although appending the flag-tag sequence to the N-terminus of TTR does not affect the kinetic or thermodynamic stability of the tetramer (*28*), this modification may affect the kinetics and/or thermodynamics of other oligomeric complexes. Isotope incorporation or the addition of fluorophores before or after subunit exchange may be more suitable for following subunit exchange in other systems utilizing mass spectrometry, FRET, or the like. Because the subunit exchange method can be readily adapted to probe kinetic stabilization of a wide range of oligomeric proteins, this strategy offers promise for the identification and development of small molecule kinetic stabilizers for numerous proteins that misfold and result in disease.

ACKNOWLEDGMENT

We would like to thank Per Hammarström, Patrick Braun, and Evan Powers for helpful discussions.

SUPPORTING INFORMATION AVAILABLE

A detailed description of the mathematical model of subunit exchange, including definitions of the various constants, the kinetic equations used for the model, and the Mathematica code used to evaluate the model. This material is available free of charge via the Internet at http://pubs.acs.org.

REFERENCES

1. Hamilton, J. A., and Benson, M. D. (2001) Transthyretin: a review from a structural perspective, *Cell Mol. Life Sci. 58*, 1491−1521.
2. Westermark, P., Sletten, K., Johansson, B., and Cornwell, G. G., 3rd. (1990) Fibril in senile systemic amyloidosis is derived from normal transthyretin, *Proc. Natl. Acad. Sci., U.S.A. 87*, 2843−2845.
3. Hammarstrom, P., Sekijima, Y., White, J. T., Wiseman, R. L., Lim, A., Costello, C. E., Altland, K., Garzuly, F., Budka, H., and Kelly, J. W. (2003) D18G transthyretin is monomeric, aggregation prone, and not detectable in plasma and cerebrospinal fluid: a prescription for central nervous system amyloidosis? *Biochemistry 42*, 6656−6663.
4. Plante-Bordeneuve, V., Lalu, T., Misrahi, M., Reilly, M. M., Adams, D., Lacroix, C., and Said, G. (1998) Genotypic-phenotypic variations in a series of 65 patients with familial amyloid polyneuropathy, *Neurology 51*, 708−714.
5. Jacobson, D. R., McFarlin, D. E., Kane, I., and Buxbaum, J. N. (1992) Transthyretin Pro55, a variant associated with early-onset, aggressive, diffuse amyloidosis with cardiac and neurologic involvement, *Hum. Genet. 89*, 353−356.
6. Sekijima, Y., Wiseman, R. L., Matteson, J., Hammarstrom, P., Miller, S. R., Sawkar, A. R., Balch, W. E., and Kelly, J. W. (2005) The Biological and Chemical Basis for Tissue Selective Amyloid Disease, *Cell 121*, 73−85.
7. Saraiva, M. J. (1995) Transthyretin mutations in health and disease, *Hum. Mutat. 5*, 191−196.
8. Holmgren, G., Ericzon, B. G., Groth, C. G., Steen, L., Suhr, O., Andersen, O., Wallin, B. G., Seymour, A., Richardson, S., Hawkins, P. N., et al. (1993) Clinical improvement and amyloid regression after liver transplantation in hereditary transthyretin amyloidosis, *Lancet 341*, 1113−1116.
9. Suhr, O. B., Ericzon, B. G., and Friman, S. (2002) Long-term follow-up of survival of liver transplant recipients with familial amyloid polyneuropathy (Portuguese type), *Liver Transpl. 8*, 787−794.
10. Ando, Y., Tanaka, Y., Nakazato, M., Ericzon, B. G., Yamashita, T., Tashima, K., Sakashita, N., Suga, M., Uchino, M., and Ando, M. (1995) Change in variant transthyretin levels in patients with familial amyloidotic polyneuropathy type I following liver transplantation, *Biochem. Biophys. Res. Commun. 211*, 354−358.
11. Hammarstrom, P., Jiang, X., Hurshman, A. R., Powers, E. T., and Kelly, J. W. (2002) Sequence-dependent denaturation energetics: A major determinant in amyloid disease diversity, *Proc. Natl. Acad. Sci., U.S.A. 99*, 16427−16432.
12. Colon, W., and Kelly, J. W. (1992) Partial denaturation of transthyretin is sufficient for amyloid fibril formation in vitro, *Biochemistry 31*, 8654−8660.
13. Lai, Z., Colon, W., and Kelly, J. W. (1996) The acid-mediated denaturation pathway of transthyretin yields a conformational intermediate that can self-assemble into amyloid, *Biochemistry 35*, 6470−6482.
14. Coelho, T., Carvalho, M., Saraiva, M. J., et al. (1993) A Strikingly Benign Evolution of FAP in an Individual Compound Heterozygote for Two TTR Mutations: TTR Met30 and TTR Met119, *J. Rheumatol. 20*, 179.
15. Hammarstrom, P., Schneider, F., and Kelly, J. W. (2001) Trans-suppression of misfolding in an amyloid disease, *Science 293*, 2459−2462.
16. Hammarstrom, P., Wiseman, R. L., Powers, E. T., and Kelly, J. W. (2003) Prevention of transthyretin amyloid disease by changing protein misfolding energetics, *Science 299*, 713−716.
17. Green, N. S., Palaninathan, S. K., Sacchettini, J. C., and Kelly, J. W. (2003) Synthesis and characterization of potent bivalent amyloidosis inhibitors that bind prior to transthyretin tetramerization, *J. Am. Chem. Soc. 125*, 13404−13414.

18. Adamski-Werner, S. L., Palaninathan, S. K., Sacchettini, J. C., and Kelly, J. W. (2004) Diflunisal analogues stabilize the native state of transthyretin. Potent inhibition of amyloidogenesis, *J. Med. Chem. 47*, 355−374.
19. Klabunde, T., Petrassi, H. M., Oza, V. B., Raman, P., Kelly, J. W., and Sacchettini, J. C. (2000) Rational design of potent human transthyretin amyloid disease inhibitors, *Nat. Struct. Biol. 7*, 312−321.
20. Miroy, G. J., Lai, Z., Lashuel, H. A., Peterson, S. A., Strang, C., and Kelly, J. W. (1996) Inhibiting transthyretin amyloid fibril formation via protein stabilization, *Proc. Natl. Acad. Sci., U.S.A. 93*, 15051−15056.
21. Oza, V. B., Smith, C., Raman, P., Koepf, E. K., Lashuel, H. A., Petrassi, H. M., Chiang, K. P., Powers, E. T., Sachettinni, J., and Kelly, J. W. (2002) Synthesis, structure, and activity of diclofenac analogues as transthyretin amyloid fibril formation inhibitors, *J. Med. Chem. 45*, 321−332.
22. Purkey, H. E., Palaninathan, S. K., Kent, K. C., Smith, C., Safe, S. H., Sacchettini, J. C., and Kelly, J. W. (2004) Hydroxylated polychlorinated biphenyls selectively bind transthyretin in blood and inhibit amyloidogenesis: rationalizing rodent PCB toxicity, *Chem. Biol. 11*, 1719−1728.
23. Razavi, H., Palaninathan, S. K., Powers, E. T., Wiseman, R. L., Purkey, H. E., Mohamedmohaideen, N. N., Deechongkit, S., Chiang, K. P., Dendle, M. T., Sacchettini, J. C., and Kelly, J. W. (2003) Benzoxazoles as transthyretin amyloid fibril inhibitors: synthesis, evaluation, and mechanism of action, *Angew. Chem., Int. Ed. 42*, 2758−2761.
24. Reixach, N., Deechongkit, S., Jiang, X., Kelly, J. W., and Buxbaum, J. N. (2004) Tissue damage in the amyloidoses: Transthyretin monomers and nonnative oligomers are the major cytotoxic species in tissue culture, *Proc. Natl. Acad. Sci., U.S.A. 101*, 2817−2822.
25. Sousa, M. M., Cardoso, I., Fernandes, R., Guimaraes, A., and Saraiva, M. J. (2001) Deposition of transthyretin in early stages of familial amyloidotic polyneuropathy: evidence for toxicity of nonfibrillar aggregates, *Am. J. Pathol. 159*, 1993−2000.
26. Lashuel, H. A., Lai, Z., and Kelly, J. W. (1998) Characterization of the transthyretin acid denaturation pathways by analytical ultracentrifugation: implications for wild-type, V30M, and L55P amyloid fibril formation, *Biochemistry 37*, 17851−17864.
27. Damas, A. M., and Saraiva, M. J. (2000) Review: TTR amyloidosis-structural features leading to protein aggregation and their implications on therapeutic strategies, *J. Struct. Biol. 130*, 290−299.
28. Schneider, F., Hammarstrom, P., and Kelly, J. W. (2001) Transthyretin slowly exchanges subunits under physiological conditions: A convenient chromatographic method to study subunit exchange in oligomeric proteins, *Protein Sci. 10*, 1606−1613.
29. Lashuel, H. A., Wurth, C., Woo, L., and Kelly, J. W. (1999) The most pathogenic transthyretin variant, L55P, forms amyloid fibrils under acidic conditions and protofilaments under physiological conditions, *Biochemistry 38*, 13560−13573.
30. Fersht, A. (1999) *Structure and Mechanism in Protein Science*, W. H. Freeman and Company, New York.
31. Foss, T. R., Kelker, M. S., Wiseman, R. L., Wilson, I. A., and Kelly, J. W. (2005) Kinetic Stabilization of the Native State by Protein Engineering: Implications of Transthyretin Amyloidogenesis, *J. Mol. Biol. 347*, 841−854.
32. Wiseman, R. L., Johnson, S. J., Kelker, M. S., Foss, T., Wilson, I. A., and Kelly, J. W. (2005) Kinetic Stabilization of an Oligomeric Protein by a Single Ligand Binding Event, *J. Am. Chem. Soc. 127*, 5540−5551.
33. Peterson, S. A., Klabunde, T., Lashuel, H. A., Purkey, H., Sacchettini, J. C., and Kelly, J. W. (1998) Inhibiting transthyretin conformational changes that lead to amyloid fibril formation, *Proc. Natl. Acad. Sci., U.S.A. 95*, 12956−12960.
34. Leavitt, S., and Freire, E. (2001) Direct measurement of protein binding energetics by isothermal titration calorimetry, *Curr. Opin. Struct. Biol. 11*, 560−566.
35. McCammon, M. G., Scott, D. J., Keetch, C. A., Greene, L. H., Purkey, H. E., Petrassi, H. M., Kelly, J. W., and Robinson, C. V. (2002) Screening transthyretin amyloid fibril inhibitors: characterization of novel multiprotein, multiligand complexes by mass spectrometry, *Structure 10*, 851−863.
36. Sacchettini, J. C., and Kelly, J. W. (2002) Therapeutic strategies for human amyloid diseases, *Nat. Rev. Drug Discovery 1*, 267−275.
37. Bruijn, L. I., Miller, T. M., and Cleveland, D. W. (2004) Unraveling the mechanisms involved in motor neuron degeneration in ALS, *Annu. Rev. Neurosci. 27*, 723−749.
38. Li, S. H., and Li, X. J. (2004) Huntingtin-protein interactions and the pathogenesis of Huntington's disease, *Trends Genet. 20*, 146−154.

BI050352O